Evidence for widespread thermal acclimation of canopy photosynthesis

nature plants

Article

https://doi.org/10.1038/s41477-024-01846-1

Evidence for widespread thermal acclimation of canopy photosynthesis

Received: 4 March 2024

Accepted: 11 October 2024

Published online: 8 November 2024

Check for updates

Jiangong Liu[1] ✉, Youngryel Ryu[1,2] ✉, Xiangzhong Luo[3], Benjamin Dechant[1,4,5], Benjamin D. Stocker[6,7], Trevor F. Keenan[8,9], Pierre Gentine[10,11], Xing Li[1], Bolun Li[1,12], Sandy P. Harrison[13,14] & Iain Colin Prentice[14,15]

Plants acclimate to temperature by adjusting their photosynthetic capacity over weeks to months. However, most evidence for photosynthetic acclimation derives from leaf-scale experiments. Here we address the scarcity of evidence for canopy-scale photosynthetic acclimation by examining the correlation between maximum photosynthetic rates ($A_{max,2,000}$) and growth temperature ($\overline{T_{air}}$) across a range of concurrent temperatures and canopy foliage quantity, using data from >200 eddy covariance sites. We detect widespread thermal acclimation of canopy-scale photosynthesis, demonstrated by enhanced $A_{max,2,000}$ under higher $\overline{T_{air}}$, across flux sites with adequate water availability. A 14-day period is identified as the most relevant timescale for acclimation across all sites, with a range of 12–25 days for different plant functional types. The mean apparent thermal acclimation rate across all ecosystems is 0.41 (−0.38–1.04 for 5th–95th percentile range) μmol m^{-2} s^{-1} $°C^{-1}$, with croplands showing the largest acclimation rates and grasslands the lowest. Incorporating an optimality-based prediction of leaf photosynthetic capacities into a biochemical photosynthesis model is shown to improve the representation of thermal acclimation. Our results underscore the critical need for enhanced understanding and modelling of canopy-scale photosynthetic capacity to accurately predict plant responses to warmer growing seasons.

The carbon uptake capacity of terrestrial ecosystem photosynthesis shows large spatiotemporal variation[1]. Air temperature (T_{air}) is one of the key factors determining this variation[2]. Given recent warming of 0.1–0.3 °C per decade[3], a better understanding of ecosystem responses to T_{air} is needed. While the instantaneous temperature dependence of photosynthesis has been a major focus of research[4–6] and is represented in vegetation and land surface models[7–9], the slower process known as thermal acclimation, through which plants maintain or enhance their photosynthetic efficiency in response to warmer growth temperatures[10–14], is less well understood[15,16]. Several studies have indicated that leaves acclimate to thermal growing conditions within weeks to months, although the relevant timescales for different plant types remain uncertain[17–20]. The potential mechanisms of this (non-genetic) acclimation include changes in key biochemical parameters (electron-transport potential and carboxylation capacity)[12,14,21], the sensitivity of stomatal conductance to atmospheric vapour pressure deficit (VPD)[22–24] and enzymatic heat tolerance[10,14].

Widespread evidence of thermal acclimation at the leaf and canopy scales indicates that the optimal temperature (T_{opt}) of photosynthesis adjusts in accordance with the prevailing T_{air} averaged over the time frame most relevant for acclimation ($\overline{T_{air}}$)[12,14,21,25,26]. Yet the extent to which the maximum carbon assimilation rate under high light (A_{max}) acclimates to $\overline{T_{air}}$ under natural conditions is less clear, particularly since most experiments are conducted on seedlings under highly

A full list of affiliations appears at the end of the paper. ✉e-mail: jl6314@columbia.edu; yryu@snu.ac.kr

controlled growth conditions[13,27]. Given that T_{opt} is well-documented to increase with rising $\overline{T_{air}}$, it is crucial to understand whether A_{max} can also acclimate to $\overline{T_{air}}$, since only their simultaneous enhancement can lead to consistent increases in photosynthesis[28,29]. While some process-based photosynthetic models have incorporated T_{opt} acclimation, A_{max} acclimation has not been adequately represented in models[30,31]. Demonstrating the presence of thermal acclimation at the canopy scale, quantifying its relevant timescales and rates across ecosystems and assessing the accuracy of photosynthetic models in representing these acclimation processes are essential for understanding how thermal acclimation can mitigate the potentially detrimental effects of warming on the future terrestrial carbon sink[16].

In this study, we define evidence for thermal acclimation of canopy photosynthesis as a positive adjustment in canopy-scale A_{max} in response to elevated $\overline{T_{air}}$. Following the definition used in leaf-scale studies[32], canopy-scale A_{max} is defined as the photosynthetic assimilation rate of the canopy measured under high light, ample water and ambient CO_2. We derive A_{max} from light response curves of half-hourly or hourly eddy covariance carbon fluxes obtained from >200 FLUXNET2015 flux sites (Methods). While canopy-scale T_{opt} has been shown to acclimate to elevated $\overline{T_{air}}$ in several previous studies[25,26,33], our focus here is solely on thermal acclimation of canopy-scale A_{max}. To facilitate consistent analysis across different light conditions, we standardize A_{max} to photosynthetic photon flux density (PPFD) equivalent to 2,000 μmol m^{-2} s^{-1} (denoted as $A_{max,2,000}$; Methods). Given the limited number of $A_{max,2,000}$ samples for individual flux sites, we infer the thermal acclimation of $A_{max,2,000}$ across spatial gradients by leveraging the large range of climates sampled by the FLUXNET2015 sites. We examine the correlation between $A_{max,2,000}$ and $\overline{T_{air}}$ when averaged over different time windows to identify the most relevant timescale (τ) for thermal acclimation, as indicated by peak correlation. Finally, we evaluate a biochemical model of canopy-scale C_3 photosynthesis[4,31], incorporating recent advances in parameterizing temperature dependence acclimation[12] and modelled optimality-based leaf photosynthetic capacity[34], to assess its ability to reproduce the observed thermal acclimation rates.

Results and discussion

Evidence for thermal acclimation of canopy photosynthesis

By binning T_{air} and the fraction of absorbed photosynthetically active radiation (fAPAR) to control for the confounding effects of concurrent temperature and seasonal changes in canopy foliage quantity and the development of the photosynthetic system on $A_{max,2,000}$, our analysis reveals a pervasive positive correlation between $A_{max,2,000}$ and $\overline{T_{air}}$ (see Methods for the derivations of τ for each plant functional type (PFT)) under conditions of adequate water availability as indicated by a high ratio of actual to potential evapotranspiration (ET/PET) (Fig. 1). This correlation is observed both spatially across multiple sites (Fig. 1a) and temporally within individual sites (Fig. 1c). We use linear mixed-effect models (LMMs) to obtain the regression coefficients of $\overline{T_{air}}$ when estimating $A_{max,2,000}$ ($A_{max,2,000} \sim \overline{T_{air}} + (1|site)$), which we define as the apparent thermal acclimation rate (γ_T, μmol CO_2 m^{-2} s^{-1} °C^{-1}). The concept of apparent rates is used here as the $A_{max,2,000}$ response rate to $\overline{T_{air}}$ may be influenced by other covarying environmental conditions[19], including the growth PPFD ($\overline{PPFD}$) and VPD[35] (Supplementary Fig. 1). To account for the potential impact of adaptation[12]—the modification of $A_{max,2,000}$–$\overline{T_{air}}$ relationships across different species and populations within a species growing at different sites—sites are treated as random intercepts within the LLMs (see Extended Data Fig. 1a for an example). Cropland sites are included in the PFT-based analyses but excluded from cross-site analyses.

Detectability of thermal acclimation in canopy photosynthesis is quantified as the percentage of T_{air}–fAPAR bins showing a positive γ_T. Our cross-site analysis for natural ecosystems finds positive γ_T values in 87% of the T_{air}–fAPAR bins (938 in total) (Fig. 1a), with 65% of these positive relationships being statistically significant ($P < 0.05$), indicating that thermal acclimation is widespread across biomes. Averaged over all T_{air}–fAPAR bins, γ_T is 0.41 ± 0.62 (mean ± s.d.) μmol CO_2 m^{-2} s^{-1} °C^{-1}, with a 5th to 95th percentile range of −0.38–1.04 μmol CO_2 m^{-2} s^{-1} °C^{-1}. The average of positive γ_T values is 0.57 ± 0.30 m^{-2} s^{-1} °C^{-1}. The PFT-based analysis also shows strong evidence of thermal acclimation, with mean γ_T values decreasing as follows: croplands (CRO, 0.81) > deciduous broadleaf forests (DBF, 0.58) > wetlands (WET, 0.57) > evergreen needle-leaf forests (ENF, 0.54) > mixed forests (MF, 0.42) > evergreen broadleaf forests (EBF, 0.39) > grasslands (GRA, 0.34) (Fig. 1b and Extended Data Fig. 3). Furthermore, 92% of FLUXNET2015 sites with observations spanning 6 years or more show positive partial correlations between $A_{max,2,000}$ and $\overline{T_{air}}$ after controlling for potential confounding factors of $\overline{PPFD}$, T_{air} and fAPAR (Fig. 1c), indicating widespread acclimation to seasonal temperature variations at individual flux sites. Sites showing a negative correlation are mainly located in the tropics (Extended Data Fig. 4a).

The potential confounding effect of factors other than $\overline{T_{air}}$ on $A_{max,2,000}$ appears to be minimal as the detectability of thermal acclimation remains high across diverse conditions. The binning approach has proved effective in previous studies for analysing relationships between variables of interest while controlling for confounding factors[35–37]. The effects of concurrent T_{air} and seasonal changes in fAPAR on $A_{max,2,000}$ under T_{air}–fAPAR bin pairs are shown to be very weak (Extended Data Fig. 1b,c). To ensure our findings are not skewed by light acclimation[35], we consider the detectability of thermal acclimation when incorporating $\overline{PPFD}$ into LLMs (89%; Extended Data Fig. 2a) and controlling for $\overline{PPFD}$ through partial correlation (85%; Extended Data Fig. 2b). The impact of VPD is probably limited, as its negative effect on A_{max} has been accounted for during the derivation of A_{max} (equation (3) in Methods) and has been further mitigated by ET/PET filtering. After filtering, there is a positive relationship between $A_{max,2,000}$ and VPD (Supplementary Fig. 1c). Any negative VPD impact on $A_{max,2,000}$ is expected to reinforce, not diminish, the observed widespread thermal acclimation. Diffuse radiation is expected to increase A_{max} by penetrating into deep canopy layers where light is limited[38,39]. However, this effect does not confound the relationship between $A_{max,2,000}$ and $\overline{T_{air}}$ (Supplementary Fig. 2) since the conditions of diffuse radiation on the days of A_{max} measurements do not necessarily show a strong positive correlation with $\overline{T_{air}}$ (Supplementary Table 1). Additionally, our findings remain robust with respect to the metric choice; detectability is 88% when A_{max} is unstandardized to a specific PPFD level and 87% when PFTs are treated as random effects within LLMs (Extended Data Fig. 2c,d).

Thermal acclimation capability can be influenced by the level and variability of $\overline{T_{air}}$, as well as by species and PFTs[27,40–42]. We observe negative effects of $\overline{T_{air}}$ on $A_{max,2,000}$ when fAPAR falls below 0.7 and T_{air} exceeds 25 °C (Fig. 1a). Limited transpiration, due to a low amount of leaves, may not cool the canopy sufficiently under elevated T_{air}, making ribulose-1,5-bisphosphate (RuBP) regeneration a limiting process for canopy photosynthesis at high canopy temperature[13]. The reduction in $A_{max,2,000}$ with $\overline{T_{air}}$ may be attributed to reduced stomatal conductance under high VPD[23] (Supplementary Fig. 3f) and/or decreased maximum quantum yield of photosystem II in response to elevated temperature[5,34,43]. Additionally, under these conditions, the range of $\overline{T_{air}}$ (the difference between the 90th and 10th percentiles; 3.8 °C) is significantly narrower than among the rest (8.4 °C) (two-tailed t-test, $P < 0.01$) (Supplementary Fig. 3b). Our site-level analyses also show that the correlation between $A_{max,2,000}$ and $\overline{T_{air}}$ is positively associated with $\overline{T_{air}}$ variability and negatively with $\overline{T_{air}}$ (Extended Data Fig. 4b,c), which aligns with previous studies indicating that plants grown under low $\overline{T_{air}}$ variability and/or high $\overline{T_{air}}$ show reduced acclimation potential[27,40,44]. Conversely, leaf-scale experiments indicate that the acclimation rates of light-saturated net assimilation rates (A_{net}) under different measurement temperatures are similar[41], suggesting a limited

https://doi.org/10.1038/s41477-024-01846-1

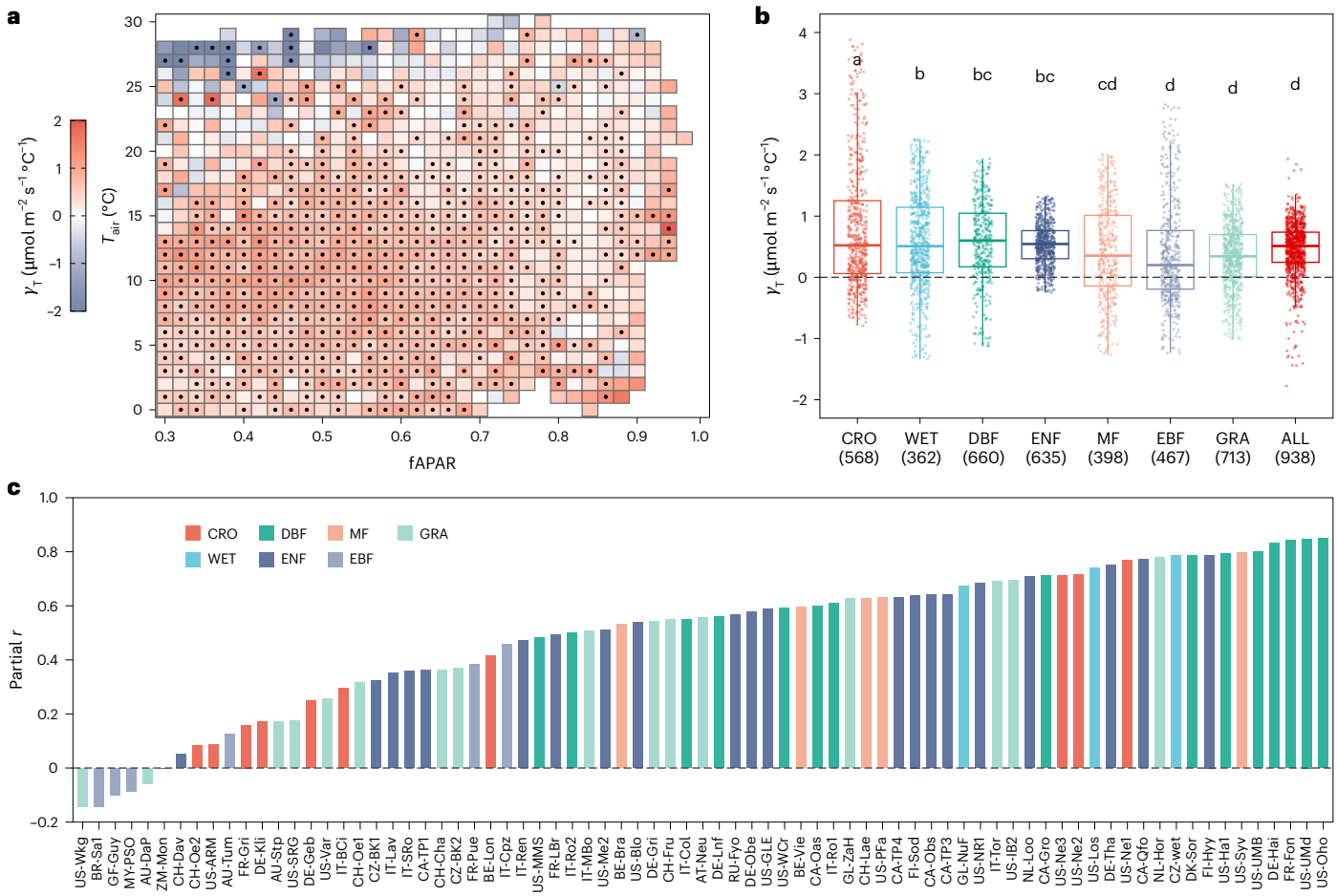

Fig. 1 | Relationships between $A_{max,2,000}$ and $\overline{T_{air}}$. **a**, γ_T values over fAPAR and T_{air} bins across flux sites. Black dots indicate significant (two-sided, $P < 0.05$) correlations between $A_{max,2,000}$ and $\overline{T_{air}}$ in the LMM ($A_{max,2,000} \approx \overline{T_{air}} + (1|site)$). **b**, PFT-specific γ_T values. PFTs are arranged in descending order on the basis of their mean γ_T values. In the box plots, the central lines represent the median γ_T values, the upper and lower box limits represent the 75th and 25th percentiles, and the upper and lower whiskers extend to 1.5 times the interquartile range, respectively. Letters represent statistically significant differences in the average γ_T values as determined by Tukey's honestly significant difference test (two-sided, $P < 0.05$), which adjusts for multiple comparisons. The numbers in parentheses represent the sample size for each PFT. **c**, Partial correlation coefficients (partial r) between $A_{max,2,000}$ and $\overline{T_{air}}$, when controlling for $\overline{PPFD}$, T_{air} and fAPAR, across individual longer-term (>5 yr) flux sites. Colours in **b** and **c** indicate different PFTs, including CRO, DBF, EBF, ENF, GRA, MF, WET and all natural biomes combined (ALL).

impact of T_{air} on $A_{max,2,000}$. Moreover, EBF is the dominant PFT for the bin pairs with high T_{air} (Supplementary Fig. 4b). There is some evidence that tropical evergreen forests have a limited capability for physiological acclimation because these forests are adapted to relatively stable thermal conditions and/or thrive under high $\overline{T_{air}}$ that is beyond the range limit for acclimation[33,45,46]. The under-representation of EBF in the FLUXNET2015 database[47] may also lead to uncertainties in the estimation of γ_T for this biome.

The observed widespread thermal acclimation of $A_{max,2,000}$ (Fig. 1) contrasts with the varying sign of the response of leaf A_{net} to $\overline{T_{air}}$, which can be positive, negative or neutral[27,40,41,48,49]. This discrepancy may stem from the fact that, unlike A_{max}, A_{net} is not necessarily measured under ample water conditions[27,32] and water stress is known to affect the capacities of plant thermal acclimation[22]. In water-limited situations, plants typically reduce water loss through transpiration by decreasing stomatal conductance[50], resulting in decreased A_{net}.

Timescale of thermal acclimation of canopy photosynthesis

The timescale for canopy photosynthetic acclimation, as measured by the correlation coefficient (r) between $A_{max,2,000}$ and $\overline{T_{air}}$ over different periods within concurrent T_{air} and fAPAR bins, varies across PFTs (Fig. 2 and Supplementary Fig. 5), increasing from GRA (12 d) to CRO (16 d), ENF (20 d), DBF (21 d) and finally WET (25 d). The τ value obtained across all sites is 14 d (Fig. 2f). For EBF, an optimal τ cannot be determined using $A_{max,2,000}$, even over an extended period of 180 d (Supplementary Fig. 5a). The enhanced vegetation index (EVI) that is derived from reflectance data in the near-infrared, red and blue spectral bands can characterize canopy structure, which closely relates with the canopy photosynthetic capacity[51]. We use a τ value of 13 d for EBF as identified by remote-sensing EVI for subsequent analysis (Methods and Supplementary Fig. 5b).

Our estimate of an average of 14 d as τ for thermal acclimation of canopy photosynthesis falls within the range of leaf-scale τ, which varies from days to months depending on species and growth conditions[10,18,20,52]. Studies that identify τ for photosynthetic acclimation using observational data across a spectrum of time frames are rare. A modelling study reports that a 15 day timescale for acclimation optimally predicts hourly eddy covariance flux measurements[53]. It is important to note that $A_{max,2,000}$ can show positive correlations with $\overline{T_{air}}$ over both the optimal τ value and other time frames close to the optimal, due to the potentially high correlation among $\overline{T_{air}}$ calculated over different short-term periods.

https://doi.org/10.1038/s41477-024-01846-1

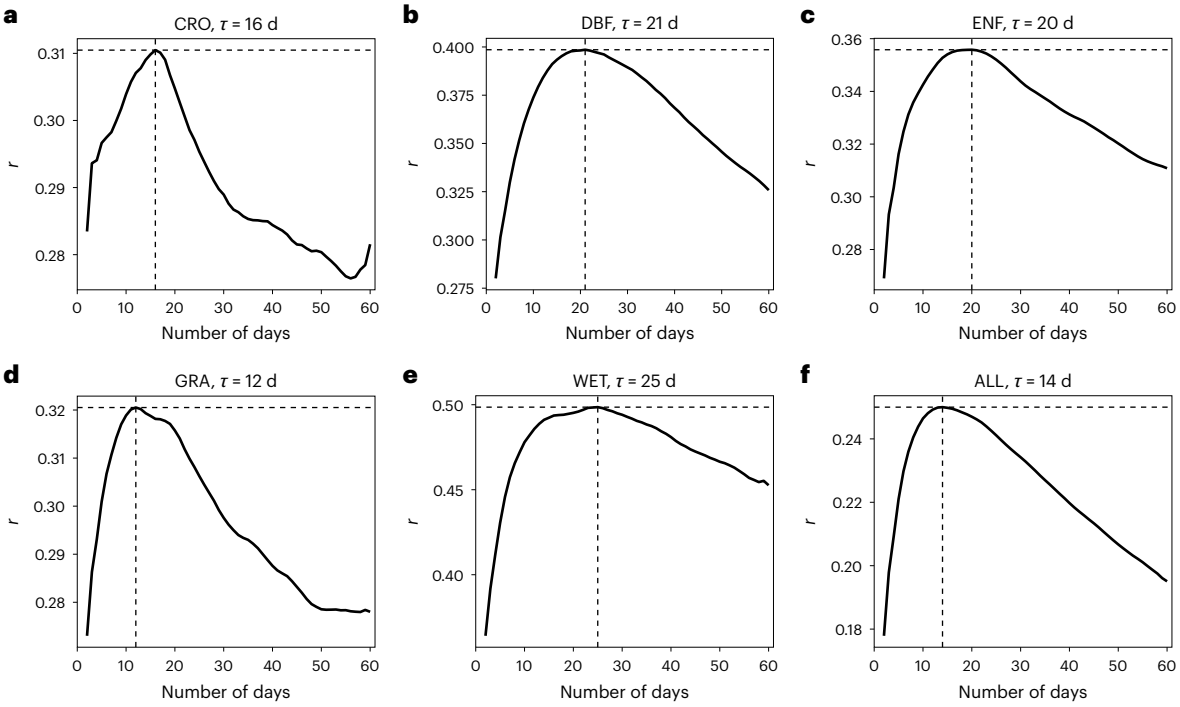

Fig. 2 | Timescales for thermal acclimation of canopy photosynthesis. **a**–**f**, The timescale for CRO (**a**), DBF (**b**), ENF (**c**), GRA (**d**), WET (**e**) and ALL (**f**). The *x* axes represent the number of days over which T_{air} is averaged to derive $\overline{T_{air}}$. The *y* axes represent the 5-day moving average of positive Pearson correlation coefficients (*r*) between $A_{max,2,000}$ and $\overline{T_{air}}$ over fAPAR and T_{air} bins. The τ value is the length of time frame for which *r* peaks.

The timescale τ for photosynthetic acclimation to a changing environment reflects a trade-off between potential benefits (for example, carbon assimilation) and costs (for example, resource re-allocation)[48]. A rapid adjustment in photosynthetic capacities is expected to enhance photosynthetic performance but is accompanied by higher costs in energy and resources[15]. The shorter τ observed in GRA and CRO are in line with the expectation that fast-growing plants with a high generation rate of new leaves might show shorter τ than slow-growing species due to their greater physiological plasticity[54]. Conversely, we found larger τ values in forests and WET, indicating that these ecosystems require more time for acclimation; however, this longer acclimation period is potentially compensated for by a higher acclimation rate (Fig. 1b). The PFT-specific and cross-site τ values for the canopy photosynthetic capacity provide a credible basis for explicitly incorporating the timescale of thermal acclimation into vegetation and land surface models.

Representing acclimation in photosynthesis models

We further explore the representation of $A_{max,2,000}$ thermal acclimation in a biochemical model for C_3 canopy photosynthesis incorporated in the Breathing Earth System Simulator (BESS)[55], based on the Farquhar–von Caemmerer–Berry (FvCB) model[4] (Methods). We test three alternative approaches, each under different resource-use allocation assumptions, to estimate maximum carboxylation rates (V_{cmax}, μmol m^{-2} s^{-1}) standardized to 25 °C (V_{cmax}^{25C}). These approaches are: (1) assuming a temporally constant and PFT-specific V_{cmax}^{25C} ($V_{cmax\_PFT}^{25C}$), where plants do not actively regulate V_{cmax}^{25C} through the growing seasons; (2) scaling leaf V_{cmax}^{25C} by canopy phenology, as indicated by leaf area index (LAI) (LAI-scaled V_{cmax}^{25C}, $V_{cmax\_LAI}^{25C}$); and (3) modelling acclimation to prevailing environments based on the eco-evolutionary optimality (EEO) theory[34,56] ($V_{cmax\_EEO}^{25C}$) (Methods and Supplementary Texts 1 and 2). The FvCB model as applied here incorporates recent advances in parameterizing the temperature dependence of leaf photosynthetic capacities to represent T_{opt} acclimation[12] (Supplementary Text 1). We run the model using the site-level forcings from the FLUXNET2015 database and derive $A_{max,2,000}$ by setting PPFD equivalent to 2,000 μmol m^{-2} s^{-1}. Canopy temperature is a key uncertainty in modelling canopy-scale photosynthesis[30,57]. We evaluate model performance using three temperature approximations, including T_{air}, aerodynamic surface temperature and radiometric surface temperature[58]. We finally use T_{air} to represent canopy temperature because it has comparable performance to the other two approximations and greater data availability (Supplementary Text 1 and Supplementary Fig. 8). For further analysis, we select estimated $A_{max,2,000}$ values from 65 C_3 sites excluding CRO and water-limited sites, where all three model variants show acceptable accuracy in estimating $A_{max,2,000}$ (coefficient of determination (R^2) > 0.5) (Supplementary Table 2).

The BESS model variant incorporating optimality-based $V_{cmax\_EEO}^{25C}$ more closely approximates the observed γ_T compared to the other two variants, $V_{cmax\_PFT}^{25C}$ ($BESS_{PFT}$) and $V_{cmax\_LAI}^{25C}$ ($BESS_{LAI}$) (Fig. 3). The Kolmogorov–Smirnov (K–S) test indicates that the cumulative distribution functions of γ_T between $BESS_{EEO}$ and FLUXNET2015 observations are more closely aligned, despite significant differences between all three BESS model distributions and observations ($P < 0.05$) (Fig. 3b). $BESS_{PFT}$ and $BESS_{LAI}$ underestimate the median observed γ_T by 65% and 50%, respectively, while $BESS_{EEO}$ overestimates it by 34% (Fig. 3a).

The considerable underestimation of γ_T by $BESS_{PFT}$ and $BESS_{LAI}$ highlights the limitation in process-based photosynthetic models that incorporate only T_{opt} acclimation. To capture γ_T accurately, process-based models must also integrate seasonal variations in photosynthetic capacities resulting from thermal acclimation. The overestimation by $BESS_{EEO}$ can be attributed to its higher predicted detectability (99%) of thermal acclimation than observed (92%) (Fig. 3a). When calculating $V_{cmax\_EEO}^{25C}$, we assume that plants are not water-stressed following ET/PET filtering; a water-stress factor is not applied to scale V_{cmax}^{25C} as described in ref. 43 (Supplementary Text 2). Consequently, in this study, the EEO theory represents an idealized condition where carbon assimilation is optimized under the assumption of sufficient water availability. While plant light use efficiency can be reduced by physiological stress due to water scarcity[59], the absence

https://doi.org/10.1038/s41477-024-01846-1

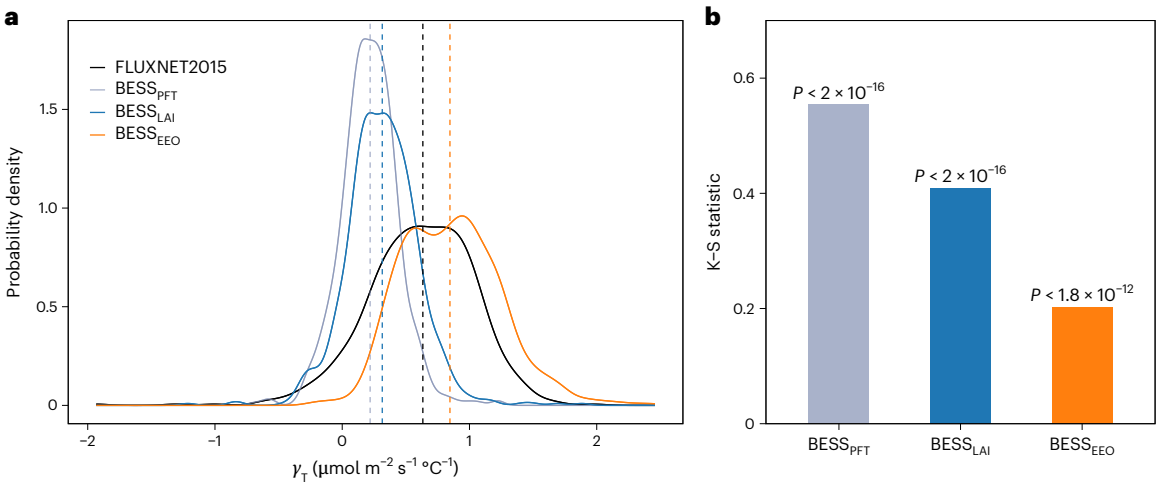

Fig. 3 | Impact of leaf photosynthetic capacities on γ_T estimation. a, Probability densities of γ_T values derived from FLUXNET2015 and three variants of the BESS model (BESS$_{PFT}$, BESS$_{LAI}$ and BESS$_{EEO}$). The vertical lines represent the median γ_T values. **b**, The statistics of the two-sided K–S tests between FLUXNET2015 observations and three model variants.

of such water-stress constraints can lead to an overestimation of V_{cmax}^{25C}. Although ET/PET is an effective indicator of soil moisture, it may not fully correspond to plant physiological stress. Bridging the gap between existing water availability metrics and actual plant stress responses remains a challenge[60].

Conclusion

Photosynthesis can benefit from future warming through thermal acclimation, resulting in increased carbon uptake under conditions where water is not limiting. While leaf-scale acclimation is widely recognized, our study shows that the positive acclimation of canopy-scale photosynthetic capacity to growth temperature is a widespread phenomenon across various terrestrial biomes. We have shown that, on average, the canopy photosynthetic capacity acclimates to the growth thermal conditions of the preceding 14 days. Incorporating seasonal acclimation of photosynthetic capacities (the maximum carboxylation rate and the maximum electron-transport rate) is critical for achieving accurate simulations of photosynthesis in response to variations in temperature at timescales of weeks to months. Despite warmer growing seasons, water availability is increasingly constrained in many regions, potentially forcing plants to reduce photosynthetic capacity as a water conservation strategy. Improving the understanding of canopy-scale photosynthetic thermal acclimation in response to future conditions characterized by warming and variable water availability is therefore important.

Methods

Global database of ecosystem-scale carbon fluxes

We derive A_{max} from >200 eddy covariance sites from the global database FLUXNET2015, which covers a wide range of geospatial locations and PFTs[47,61] (Supplementary Table 2). FLUXNET2015 is an openly accessible database containing data on the net exchange of carbon (NEE), water and energy between the atmosphere and the biosphere and meteorological observations. Uniform processing approaches are implemented for the flux calculation and quality control across the sites[47]. We use half-hourly or hourly NEE (NEE_VUT_USTAR50), its corresponding estimation of the uncertainty caused by friction velocity filtering (NEE_VUT_USTAR50_RANDUNC) and gap-filled meteorological observations, including incoming radiation (SW_IN_F), air temperature (TA_F) and VPD (VPD_F) to derive A_{max} (refs. 47,62) (described below). Sites are excluded if data are unavailable during the MODIS period from 2002 onwards (for example, US-LWW and US-Me4) or if the uncertainty estimation is missing (for example, CA-Man).

Derivation of ecosystem-scale A_{max}

We derive A_{max} from light response curves across the FLUXNET2015 sites according to the daytime flux partitioning methods detailed in refs. 35,[63]. We fit NEE using the following hyperbolic equation:

$$-\mathrm{NEE} = \frac{\alpha\beta R_g}{\alpha R_g + \beta} + \gamma \quad (1)$$

where β (μmol CO_2 m^{-2} s^{-1}) is the target variable of interest. Variables α, R_g and γ represent the ecosystem-scale quantum yield (μmol C J^{-1}), global radiation (W m^{-2}) and ecosystem respiration (μmol CO_2 m^{-2} s^{-1}), respectively.

To account for the potential influence of high VPD (hPa), β is scaled using an exponential function only when VPD exceeds 10 hPa. Thus, we obtain A_{max} as follows:

$$A_{max} = \begin{cases} \beta, \mathrm{VPD} \le 10\ \mathrm{hPa} \\ \beta \exp\left(-k\left(\mathrm{VPD} - 10\right)\right), \mathrm{VPD} > 10\ \mathrm{hPa} \end{cases} \quad (2)$$

where β and k are fit parameters to the flux data. The ecosystem respiration term in equation (1), γ, is estimated using an Arrhenius-type function describing the temperature dependence of γ (ref. 64), which is applied to night-time data by assuming that night-time NEE is equivalent to ecosystem respiration:

$$\mathrm{NEE} = R_{ref} \exp\left\{E_0\left(\frac{1}{T_{ref} - T_0} - \frac{1}{T_{air} - T_0}\right)\right\} \quad (3)$$

where R_{ref} and E_0 are the basal respiration rate (μmol CO_2 m^{-2} s^{-1}) at a reference temperature (T_{ref} = 15 °C) and temperature sensitivity (°C), respectively. T_0 is a constant equal to −46.02 °C (ref. 65).

In practice, E_0 is first estimated according to equation (3). With a fixed E_0, the remaining parameters of equations (2) and (3) (α, β, k and R_{ref}) are derived using a time window of 2–14 d. The specific time window depends on data availability and the A_{max} value is assumed invariant within the same fitting window. On average, 25% of estimated A_{max} values are flagged as medium or low quality because the parameter ranges are unreasonable and/or the curve fitting is unconstrained (Supplementary Fig. 6b) and are subsequently discarded[35]. Additionally, A_{max} values that are constant for 14 consecutive days or more are excluded. More than 88% of the A_{max} values in the remaining dataset are fitted within a 2 d window (Supplementary Fig. 6a), indicating a

sufficient sample size for most fitting. Here we derive A_{max} using the REddyProc R package (https://github.com/bgctw/REddyProc)[66], as A_{max} is not provided in the FLUXNET2015 database. We convert PPFD to R_g using a constant of 2.1 µmol J^{-1} (ref. 67). We standardize A_{max} to PPFD = 2,000 µmol m^{-2} s^{-1} ($A_{max,2,000}$) by setting R_g = 952 W m^{-2} in equation (1) and calculating the corresponding assimilation rate. This approach can avoid any A_{max} values obtained from potentially unsaturated light conditions and ensure consistent levels of absorbed PAR[35].

Timescale for thermal acclimation of $A_{max,2,000}$

We hypothesize that the most relevant timescale for thermal acclimation (τ) ranges between 2 and 60 d, according to the coordination hypothesis and observations[18,20,68]. We conduct linear regressions between $A_{max,2,000}$ derived from the FLUXNET2015 sites and the daytime $\overline{T_{air}}$ averaged over the 2–60 d before the time of $A_{max,2,000}$ measurements with a time interval of 1 d. On the basis of a previous study[35], savanna and shrubland sites are excluded from the analysis because they are frequently subject to water stress. Croplands are excluded from the cross-site analysis. Furthermore, we exclude the $A_{max,2,000}$–$\overline{T_{air}}$ pairs collected during water-limited conditions, as indicated by the ratio of prevailing actual evapotranspiration to Priestley–Taylor potential evapotranspiration (ET/PET) < 0.7 (ref. 69) and VPD > 20 hPa. Additionally, we only focus on growing seasons, characterized by fAPAR > 0.3 and T_{air} and $\overline{T_{air}}$ > 0 °C. Daily fAPAR and LAI for each site were derived by interpolating the 8 d MODIS MOD15A2H products following ref. 35. Low-quality data affected by cloud contamination are removed[31]. A total of 149,403 $A_{max,2,000}$ records are used for further analyses.

To remove the potential effects of concurrent T_{air} and fAPAR on $A_{max,2,000}$, we group $A_{max,2,000}$–$\overline{T_{air}}$ pairs into different bins of T_{air} with 1 °C intervals and fAPAR with 0.02 intervals. This approach allows the analysis of changes in $A_{max,2,000}$ along $\overline{T_{air}}$ gradients to be made while controlling for the instantaneous temperature dependence of photosynthesis and seasonal changes in leaf quantity and the development of the photosynthetic system. Pearson r between $A_{max,2,000}$ and $\overline{T_{air}}$ that is averaged over different time frames (that is, 2–60 d with 1 d interval) is calculated for T_{air} and fAPAR bins. A positive r indicates the thermal acclimation potential of $A_{max,2,000}$. Only bins with sampling numbers larger than 10 and 20 for PFT-based and cross-site analyses, respectively, are retained. We examine the relationship between the average of the positive r values obtained from T_{air} and fAPAR bins and the time frames used to calculate $\overline{T_{air}}$ for each PFT and cross sites (Fig. 2). Parameter τ is defined as the corresponding time frame when the 5 d moving average of the positive r reaches its peak. EVI, derived from MODIS reflectance data (MCD43A4) in the near-infrared, red and blue spectral bands[51], is used to estimate τ for EBF for subsequent analysis, as an optimal τ cannot be identified for this PFT using $A_{max,2,000}$ (Supplementary Fig. 5).

Evidence for thermal acclimation of $A_{max,2,000}$

We use PFT-specific τ values for aggregating prevailing T_{air} to obtain $\overline{T_{air}}$ (Fig. 1). We run LMMs, which include a random effect of different sites for removing the site-level adaptation effect, to explore the relationship between $A_{max,2,000}$ and PFT-specific $\overline{T_{air}}$ (that is, $A_{max,2,000} \sim \overline{T_{air}} + (1|site)$) (Extended Data Fig. 1a). The same data selection procedure and T_{air} and fAPAR binning scheme are used for the cross-site analysis (Fig. 1a and see earlier). The coefficient of $\overline{T_{air}}$ estimated from LMMs is defined as thermal acclimation rate (γ_T). The sampling number, conditional and marginal correlation coefficients for the cross-site analysis are shown in Supplementary Fig. 6. The LMM is conducted with the R package lme4 (ref. 70). For each site, the sampling number of $A_{max,2,000}$–$\overline{T_{air}}$ pairs is insufficient to support the correlation analysis under the binning scheme[35]. Instead, a partial correlation analysis is run between $A_{max,2,000}$ and $\overline{T_{air}}$ controlling for $\overline{PPFD}$, T_{air} and fAPAR on flux sites with observation lengths longer than 5 yr (Fig. 1c).

The prevailing conditions of T_{air} and PPFD often show a high correlation (Supplementary Fig. 1a). Therefore, we also include $\overline{PPFD}$ as an additional predictor in the LMM (Extended Data Fig. 2a) and we analyse partial correlations between $A_{max,2,000}$ and $\overline{T_{air}}$ controlling for $\overline{PPFD}$ (Extended Data Fig. 2b) to eliminate the confounding effect of light acclimation[35]. Additionally, we repeat LMMs with a different target variable (A_{max}) and random effect (PFT) to examine the robustness of the detectability of thermal acclimation (Extended Data Fig. 2c,d).

Modelling canopy photosynthesis of C_3 plants

We apply the photosynthesis module of the BESS model[57] to estimate canopy photosynthesis (A) and subsequently $A_{max,2,000}$, for each flux site. This allows a direct comparison to be made of the impacts of different empirical formulations of leaf photosynthetic capacities on thermal acclimation. The photosynthesis module is based on the FvCB model[4], where A is determined as the lower CO_2 assimilation rate between the maximum rate of ribulose-1,5-bisphosphate carboxylase/oxygenase activity when light is saturated (A_c) and the electron-transport rate for RuBP regeneration when light is limited (A_j). For this study, the two-big-leaf scheme implemented in the BESS model is simplified to a one-big-leaf scheme. We have updated the parameters of temperature dependence of the maximum carboxylation rate (V_{cmax}, µmol m^{-2} s^{-1}), the maximum electron-transport rate (J_{max}, µmol m^{-2} s^{-1}), as well as the ratio of their values at 25 °C following ref. 12. A detailed description of the canopy photosynthesis model can be found in Supplementary Text 1 (also see refs. 31,55,57).

Leaf photosynthetic capacities

V_{cmax} is a key parameter in the FvCB model, particularly under light-saturated conditions[4]. Previous studies have shown that leaf biochemical components can acclimate to $\overline{T_{air}}$ (refs. 11,12,21). In this study, we compare three empirically derived variants of V_{cmax} at 25 °C (V_{cmax}^{25C}) within the FvCB model to evaluate their effectiveness in simulating the observed γ_T:

(1) $V_{cmax\_PFT}^{25C}$: this variant assumes a constant V_{cmax}^{25C} value over the growing season, an assumption that is still widely used in vegetation models[16]. The prescribed top leaf V_{cmax}^{25C} values are adopted from a look-up table based on PFTs and climatic zones compiled from the TRY trait database[31,71].

(2) $V_{cmax\_LAI}^{25C}$: leaf V_{cmax}^{25C} varies seasonally, with its seasonality following LAI. This scheme, implemented in the previous version of the BESS model[31], follows equation (4).

$$V_{cmax\_LAI}^{25C} = a \times V_{cmax\_PFT}^{25C} + (1-a) \times V_{cmax\_PFT}^{25C} \times \frac{LAI - LAI_{min}}{LAI_{max} - LAI_{min}} \quad (4)$$

where LAI_{min} and LAI_{max} are the 5th and 95th percentile values of LAI over a growing season, respectively, and a is an empirical parameter set to 0.3 (ref. 57).

(3) $V_{cmax\_EEO}^{25C}$: the calculation is based on EEO theory[19,34,56], specifically the coordination hypothesis[17,72] and the least-cost hypothesis[50,73]. The coordination hypothesis proposes that plants actively coordinate resource allocation so that A_c tends to equal A_j on weekly to monthly timescales. The least-cost hypothesis proposes that plants minimize the combined costs (per unit assimilation) of maintaining the biochemical capacity for photosynthesis and the water transport capacity required to support it, through stomatal regulation. Combining the two hypotheses results in an optimal intercellular CO_2 concentration under representative conditions[74]. Here we assume that $V_{cmax\_EEO}^{25C}$ acclimates to prevailing conditions following the same timescale as $A_{max,2,000}$ (Fig. 2). The calculation is detailed in Supplementary Text 2 and ref. 34.

Reporting summary
Further information on research design is available in the Nature Portfolio Reporting Summary linked to this article.

Data availability
The dataset of FLUXNET2015 flux sites under the CC-BY-4.0 policy is publicly available for download at http://fluxnet.fluxdata.org. Remote-sensing canopy structure data from the MODIS MCD43A and MOD15A2H products are freely accessible at https://lpdaac.usgs.gov/products/mcd43a3v006/ and https://lpdaac.usgs.gov/products/mod15a2hv006/. BESS flux products are publicly available at https://www.environment.snu.ac.kr/data/.

Code availability
The corresponding R code scripts used in this study are available via Zenodo at https://doi.org/10.5281/zenodo.13854273 (ref. 75). The code for the deviation of A_{max} from the FLUXNET2015 database is available via GitHub at https://github.com/trevorkeenan/inhibitionPaperCode. The code for modelling optimality-based V_{cmax} is available via GitHub at https://github.com/chongya/SVOM.

References

1. Anav, A. et al. Spatiotemporal patterns of terrestrial gross primary production: a review. *Rev. Geophys.* **53**, 785–818 (2015).
2. Beer, C. et al. Terrestrial gross carbon dioxide uptake: global distribution and covariation with climate. *Science* **329**, 834–838 (2010).
3. IPCC *Special Report on Impacts of Global Warming of 1.5 °C* (eds Masson-Delmotte, V. et al.) (Cambridge Univ. Press, 2022).
4. Farquhar, G. D., von Caemmerer, S. & Berry, J. A. A biochemical model of photosynthetic CO_2 assimilation in leaves of C_3 species. *Planta* **149**, 78–90 (1980).
5. Bernacchi, C. J., Singsaas, E. L., Pimentel, C., Portis, A. R. & Long, S. P. Improved temperature response functions for models of Rubisco-limited photosynthesis. *Plant Cell Environ.* **24**, 253–259 (2001).
6. Sage, R. F. & Kubien, D. S. The temperature response of C_3 and C_4 photosynthesis. *Plant Cell Environ.* **30**, 1086–1106 (2007).
7. Bernacchi, C. J. et al. Modelling C_3 photosynthesis from the chloroplast to the ecosystem. *Plant Cell Environ.* **36**, 1641–1657 (2013).
8. Mercado, L. M. et al. Large sensitivity in land carbon storage due to geographical and temporal variation in the thermal response of photosynthetic capacity. *New Phytol.* **218**, 1462–1477 (2018).
9. Oliver, R. J. et al. Improved representation of plant physiology in the JULES-vn5.6 land surface model: photosynthesis, stomatal conductance and thermal acclimation. *Geosci. Model. Dev.* **15**, 5567–5592 (2022).
10. Berry, J. & Bjorkman, O. Photosynthetic response and adaptation to temperature in higher plants. *Annu. Rev. Plant Physiol.* **31**, 491–543 (1980).
11. Medlyn, B. E. et al. Temperature response of parameters of a biochemically based model of photosynthesis. II. A review of experimental data. *Plant Cell Environ.* **25**, 1167–1179 (2002).
12. Kumarathunge, D. P. et al. Acclimation and adaptation components of the temperature dependence of plant photosynthesis at the global scale. *New Phytol.* **222**, 768–784 (2019).
13. Crous, K. Y., Uddling, J. & De Kauwe, M. G. Temperature responses of photosynthesis and respiration in evergreen trees from boreal to tropical latitudes. *New Phytol.* **234**, 353–374 (2022).
14. Yamori, W., Hikosaka, K. & Way, D. A. Temperature response of photosynthesis in C_3, C_4, and CAM plants: temperature acclimation and temperature adaptation. *Photosynth. Res.* **119**, 101–117 (2014).
15. Dietze, M. C. Gaps in knowledge and data driving uncertainty in models of photosynthesis. *Photosynth. Res.* **119**, 3–14 (2014).
16. Rogers, A. et al. A roadmap for improving the representation of photosynthesis in Earth system models. *New Phytol.* **213**, 22–42 (2017).
17. Maire, V. et al. The coordination of leaf photosynthesis links C and N fluxes in C_3 plant species. *PLoS ONE* **7**, e38345 (2012).
18. Smith, N. G. & Dukes, J. S. Drivers of leaf carbon exchange capacity across biomes at the continental scale. *Ecology* **99**, 1610–1620 (2018).
19. Smith, N. G. et al. Global photosynthetic capacity is optimized to the environment. *Ecol. Lett.* **22**, 506–517 (2019).
20. Smith, N. G. & Dukes, J. S. Short-term acclimation to warmer temperatures accelerates leaf carbon exchange processes across plant types. *Glob. Change Biol.* **23**, 4840–4853 (2017).
21. Kattge, J. & Knorr, W. Temperature acclimation in a biochemical model of photosynthesis: a reanalysis of data from 36 species. *Plant Cell Environ.* **30**, 1176–1190 (2007).
22. Lin, Y. S., Medlyn, B. E. & Ellsworth, D. S. Temperature responses of leaf net photosynthesis: the role of component processes. *Tree Physiol.* **32**, 219–231 (2012).
23. Grossiord, C. et al. Plant responses to rising vapor pressure deficit. *New Phytol.* **226**, 1550–1566 (2020).
24. López, J., Way, D. A. & Sadok, W. Systemic effects of rising atmospheric vapor pressure deficit on plant physiology and productivity. *Glob. Change Biol.* **27**, 1704–1720 (2021).
25. Niu, S. et al. Thermal optimality of net ecosystem exchange of carbon dioxide and underlying mechanisms. *New Phytol.* **194**, 775–783 (2012).
26. Baldocchi, D. et al. FLUXNET: a new tool to study the temporal and spatial variability of ecosystem-scale carbon dioxide, water vapor, and energy flux densities. *Bull. Am. Meteorol. Soc.* **82**, 2415–2434 (2001).
27. Vico, G., Way, D. A., Hurry, V. & Manzoni, S. Can leaf net photosynthesis acclimate to rising and more variable temperatures? *Plant Cell Environ.* **42**, 1913–1928 (2019).
28. Way, D. A. & Yamori, W. Thermal acclimation of photosynthesis: on the importance of adjusting our definitions and accounting for thermal acclimation of respiration. *Photosynth. Res.* **119**, 89–100 (2014).
29. Dusenge, M. E. et al. Boreal conifers maintain carbon uptake with warming despite failure to track optimal temperatures. *Nat. Commun.* **14**, 4667 (2023).
30. Knauer, J. et al. Higher global gross primary productivity under future climate with more advanced representations of photosynthesis. *Sci. Adv.* **9**, eadh9444 (2023).
31. Jiang, C. & Ryu, Y. Multi-scale evaluation of global gross primary productivity and evapotranspiration products derived from Breathing Earth System Simulator (BESS). *Remote Sens. Environ.* **186**, 528–547 (2016).
32. Wright, I. J. et al. The worldwide leaf economics spectrum. *Nature* **428**, 821–827 (2004).
33. Huang, M. et al. Air temperature optima of vegetation productivity across global biomes. *Nat. Ecol. Evol.* **3**, 772–779 (2019).
34. Jiang, C., Ryu, Y., Wang, H. & Keenan, T. F. An optimality-based model explains seasonal variation in C_3 plant photosynthetic capacity. *Glob. Change Biol.* **26**, 6493–6510 (2020).
35. Luo, X. & Keenan, T. F. Global evidence for the acclimation of ecosystem photosynthesis to light. *Nat. Ecol. Evol.* **4**, 1351–1357 (2020).
36. Liu, L. et al. Soil moisture dominates dryness stress on ecosystem production globally. *Nat. Commun.* **11**, 4892 (2020).
37. Novick, K. A. et al. The increasing importance of atmospheric demand for ecosystem water and carbon fluxes. *Nat. Clim. Change* **6**, 1023–1027 (2016).

38. Zhou, H. et al. Responses of gross primary productivity to diffuse radiation at global FLUXNET sites. *Atmos. Environ.* **244**, 117905 (2021).
39. Mercado, L. M. et al. Impact of changes in diffuse radiation on the global land carbon sink. *Nature* **458**, 1014–1017 (2009).
40. Sendall, K. M. et al. Acclimation of photosynthetic temperature optima of temperate and boreal tree species in response to experimental forest warming. *Glob. Change Biol.* **21**, 1342–1357 (2015).
41. Battaglia, M., Beadle, C. & Loughhead, S. Photosynthetic temperature responses of *Eucalyptus globulus* and *Eucalyptus nitens*. *Tree Physiol.* **16**, 81–89 (1996).
42. Slot, M., Rifai, S. W. & Winter, K. Photosynthetic plasticity of a tropical tree species, *Tabebuia rosea*, in response to elevated temperature and [CO_2]. *Plant Cell Environ.* **44**, 2347–2364 (2021).
43. Stocker, B. D. et al. P-model v1.0: an optimality-based light use efficiency model for simulating ecosystem gross primary production. *Geosci. Model. Dev.* **13**, 1545–1581 (2020).
44. Luo, Y., Gessler, A., D'Odorico, P., Hufkens, K. & Stocker, B. D. Quantifying effects of cold acclimation and delayed springtime photosynthesis resumption in northern ecosystems. *New Phytol.* **240**, 984–1002 (2023).
45. Dusenge, M. E. et al. Limited thermal acclimation of photosynthesis in tropical montane tree species. *Glob. Change Biol.* **27**, 4860–4878 (2021).
46. Doughty, C. E. et al. Tropical forests are approaching critical temperature thresholds. *Nature* **621**, 105–111 (2023).
47. Pastorello, G. et al. The FLUXNET2015 dataset and the ONEFlux processing pipeline for eddy covariance data. *Sci. Data* **7**, 225 (2020).
48. Smith, N. G., McNellis, R. & Dukes, J. S. No acclimation: instantaneous responses to temperature maintain homeostatic photosynthetic rates under experimental warming across a precipitation gradient in *Ulmus americana*. *AoB PLANTS* **12**, plaa027 (2020).
49. Cunningham, S. C. & Read, J. Do temperate rainforest trees have a greater ability to acclimate to changing temperatures than tropical rainforest trees? *New Phytol.* **157**, 55–64 (2003).
50. Prentice, I. C., Dong, N., Gleason, S. M., Maire, V. & Wright, I. J. Balancing the costs of carbon gain and water transport: testing a new theoretical framework for plant functional ecology. *Ecol. Lett.* **17**, 82–91 (2014).
51. Zeng, Y. et al. Optical vegetation indices for monitoring terrestrial ecosystems globally. *Nat. Rev. Earth Environ.* **3**, 477–493 (2022).
52. Mäkelä, A. et al. Developing an empirical model of stand GPP with the LUE approach: analysis of eddy covariance data at five contrasting conifer sites in Europe. *Glob. Change Biol.* **14**, 92–108 (2008).
53. Mengoli, G. et al. Ecosystem photosynthesis in land-surface models: a first-principles approach incorporating acclimation. *J. Adv. Model Earth Syst.* **14**, e2021MS002767 (2022).
54. Loveys, B. R. et al. Thermal acclimation of leaf and root respiration: an investigation comparing inherently fast- and slow-growing plant species. *Glob. Change Biol.* **9**, 895–910 (2003).
55. Li, B. et al. BESSv2.0: a satellite-based and coupled-process model for quantifying long-term global land–atmosphere fluxes. *Remote Sens. Environ.* **295**, 113696 (2023).
56. Harrison, S. P. et al. Eco-evolutionary optimality as a means to improve vegetation and land-surface models. *New Phytol.* **231**, 2125–2141 (2021).
57. Ryu, Y. et al. Integration of MODIS land and atmosphere products with a coupled-process model to estimate gross primary productivity and evapotranspiration from 1 km to global scales. *Glob. Biogeochem. Cycles* https://doi.org/10.1029/2011GB004053 (2011).
58. Knauer, J., El-Madany, T. S., Zaehle, S. & Migliavacca, M. Bigleaf—an R package for the calculation of physical and physiological ecosystem properties from eddy covariance data. *PLoS ONE* **13**, e0201114 (2018).
59. Stocker, B. D. et al. Quantifying soil moisture impacts on light use efficiency across biomes. *New Phytol.* **218**, 1430–1449 (2018).
60. Lian, X. et al. Multifaceted characteristics of dryland aridity changes in a warming world. *Nat. Rev. Earth Environ.* **2**, 232–250 (2021).
61. Baldocchi, D., Chu, H. & Reichstein, M. Inter-annual variability of net and gross ecosystem carbon fluxes: a review. *Agric. For. Meteorol.* **249**, 520–533 (2018).
62. Lasslop, G. et al. Separation of net ecosystem exchange into assimilation and respiration using a light response curve approach: critical issues and global evaluation. *Glob. Change Biol.* **16**, 187–208 (2010).
63. Keenan, T. F. et al. Widespread inhibition of daytime ecosystem respiration. *Nat. Ecol. Evol.* **3**, 407–415 (2019).
64. Papale, D. et al. Towards a standardized processing of Net Ecosystem Exchange measured with eddy covariance technique: algorithms and uncertainty estimation. *Biogeosciences* **3**, 571–583 (2006).
65. Lloyd, J. & Taylor, J. A. On the temperature dependence of soil respiration. *Funct. Ecol.* **8**, 315 (1994).
66. Wutzler, T. et al. Basic and extensible post-processing of eddy covariance flux data with REddyProc. *Biogeosciences* **15**, 5015–5030 (2018).
67. Meek, D. W., Hatfield, J. L., Howell, T. A., Idso, S. B. & Reginato, R. J. A generalized relationship between photosynthetically active radiation and solar radiation. *Agron. J.* **76**, 939–945 (1984).
68. Gunderson, C. A., O'hara, K. H., Campion, C. M., Walker, A. V. & Edwards, N. T. Thermal plasticity of photosynthesis: the role of acclimation in forest responses to a warming climate. *Glob. Change Biol.* **16**, 2272–2286 (2010).
69. Fisher, J. B., Whittaker, R. J. & Malhi, Y. ET come home: potential evapotranspiration in geographical ecology. *Glob. Ecol. Biogeogr.* **20**, 1–18 (2011).
70. Bates, D., Mächler, M., Bolker, B. & Walker, S. Fitting linear mixed-effects models using lme4. *J. Stat. Softw.* **67**, 1–48 (2015).
71. Kattge, J. et al. TRY—a global database of plant traits. *Glob. Change Biol.* **17**, 2905–2935 (2011).
72. Chen, J. L., Reynolds, J. F., Harley, P. C. & Tenhunen, J. D. Coordination theory of leaf nitrogen distribution in a canopy. *Oecologia* **93**, 63–69 (1993).
73. Wright, I. J., Reich, P. B. & Westoby, M. Least-cost input mixtures of water and nitrogen for photosynthesis. *Am. Nat.* **161**, 98–111 (2003).
74. Wang, H. et al. Towards a universal model for carbon dioxide uptake by plants. *Nat. Plants* **3**, 734–741 (2017).
75. Liu, J. Evidence for widespread thermal acclimation of canopy photosynthesis. *Zenodo* https://doi.org/10.5281/zenodo.13854273 (2024).

Acknowledgements

This research is a contribution to the LEMONTREE (land ecosystem models based on new theory, observation and experiments) project, funded through the generosity of E. and W. Schmidt by recommendation of the Schmidt Futures programme. It is also a contribution to USMILE European Research Council grant. Y.R. was supported by the Ministry of Environment of Korea (202300218237). B.D.S. was funded by the Swiss National Science Foundation grant no. PCEFP2_181115. B.D. was supported by sDiv, the Synthesis Centre of the German Centre for Integrative Biodiversity Research (iDiv) Halle-Jena-Leipzig (DFG FZT 118, 202548816). T.F.K. acknowledges additional support from a NASA Carbon Cycle Science Award

80NSSC21K1705, a US Department of Energy Early Career Research Program award no. DE-SC0021023 and the RUBISCO SFA, which is sponsored by the Regional and Global Model Analysis Program in the Climate and Environmental Sciences Division of the Office of Biological and Environmental Research in the US DOE Office of Science. X. Luo was supported by National University of Singapore Presidential Young Professorship (A-0003625-01-00). I.C.P. acknowledges funding from the European Research Council under the European Union's Horizon 2020 research and innovation programme (grant agreement no. 787203 REALM). We especially thank the researchers and contributors of the FLUXNET community and the MODIS products. We also acknowledge X. Lian and J. Fang for their helpful reviews and comments on this paper before its submission.

Author contributions

J.L. designed the study, performed the analysis and drafted the initial paper. J.L., Y.R., X. Luo, T.F.K. and P.G. participated in the early-stage discussion. I.C.P. substantially revised the paper. All co-authors commented on the results and contributed to the writing of the paper.

Competing interests

The authors declare no competing interests.

Additional information

Extended data is available for this paper at https://doi.org/10.1038/s41477-024-01846-1.

Supplementary information The online version contains supplementary material available at https://doi.org/10.1038/s41477-024-01846-1.

Correspondence and requests for materials should be addressed to Jiangong Liu or Youngryel Ryu.

Peer review information *Nature Plants* thanks Mirindi Eric Dusenge, Marc Peaucelle and the other, anonymous, reviewer(s) for their contribution to the peer review of this work.

[1]Research Institute of Agriculture and Life Sciences, Seoul National University, Seoul, Republic of Korea. [2]Department of Landscape Architecture and Rural Systems Engineering, Seoul National University, Seoul, Republic of Korea. [3]Department of Geography, National University of Singapore, Singapore, Singapore. [4]German Centre for Integrative Biodiversity Research (iDiv) Halle-Jena-Leipzig, Leipzig, Germany. [5]Leipzig University, Leipzig, Germany. [6]Institute of Geography, University of Bern, Bern, Switzerland. [7]Oeschger Centre for Climate Change Research, University of Bern, Bern, Switzerland. [8]Climate and Ecosystem Sciences Division, Lawrence Berkeley National Laboratory, Berkeley, CA, USA. [9]Department of Environmental Science, Policy, and Management, University of California, Berkeley, CA, USA. [10]Earth and Environmental Engineering Department, Columbia University, New York, NY, USA. [11]Climate School, Columbia University, New York, NY, USA. [12]School of Geographical Sciences, Nanjing University of Information Science and Technology, Nanjing, China. [13]School of Archaeology, Geography and Environmental Science (SAGES), University of Reading, Reading, UK. [14]Department of Earth System Science, Ministry of Education Key Laboratory for Earth System Modeling, Institute for Global Change Studies, Tsinghua University, Beijing, China. [15]Georgina Mace Centre for the Living Planet, Department of Life Sciences, Imperial College London, Ascot, UK. ✉e-mail: jl6314@columbia.edu; yryu@snu.ac.kr

https://doi.org/10.1038/s41477-024-01846-1

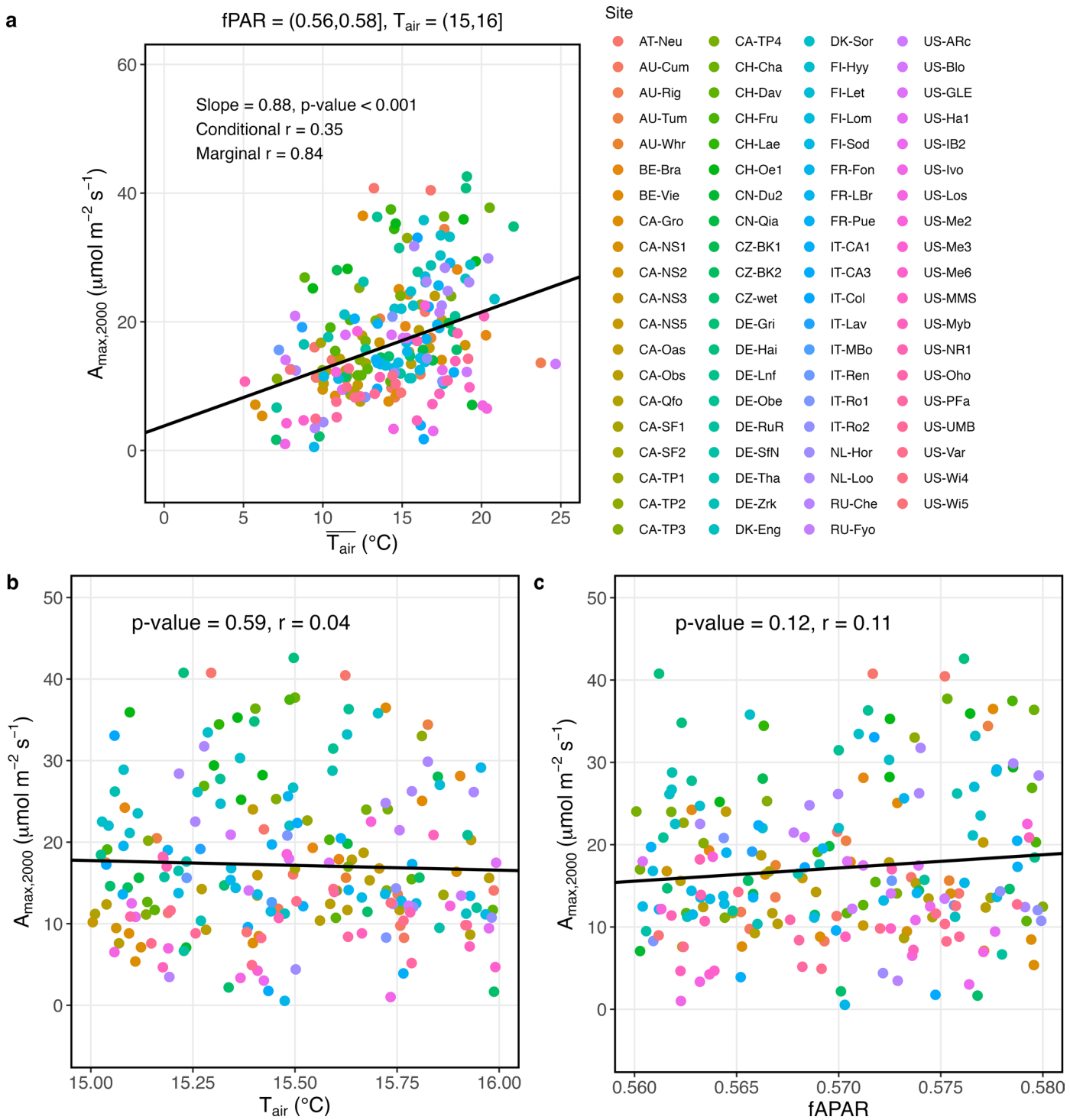

Extended Data Fig. 1 | An example of the response of $A_{max,2000}$ to $\overline{T_{air}}$, T_{air}, and fAPAR under a fAPAR-T_{air} bin pair. Cross-site $A_{max,2000}$, $\overline{T_{air}}$, T_{air}, and fAPAR samples are collected when $0.56 < fAPAR \leq 0.58$ and $15\,°C < T_{air} \leq 16\,°C$. **a**–**c**, Relationships between $A_{max,2000}$ and $\overline{T_{air}}$ (**a**), $A_{max,2000}$ and T_{air} (**b**), and $A_{max,2000}$ and fAPAR (**c**). The black lines represent the best fits between $A_{max,2000}$ and $\overline{T_{air}}$ as a linear mixed-effect function ($A_{max,2000} \sim \overline{T_{air}} + (1|Site)$, two-sided test, $P < 0.001$) (**a**), $A_{max,2000}$ and T_{air} as a linear function ($A_{max,2000} \sim T_{air}$, two-sided test, $P > 0.05$) (**b**), and $A_{max,2000}$ and fAPAR as a linear function ($A_{max,2000} \sim$ fAPAR, two-sided test, $P > 0.05$) (**c**).

https://doi.org/10.1038/s41477-024-01846-1

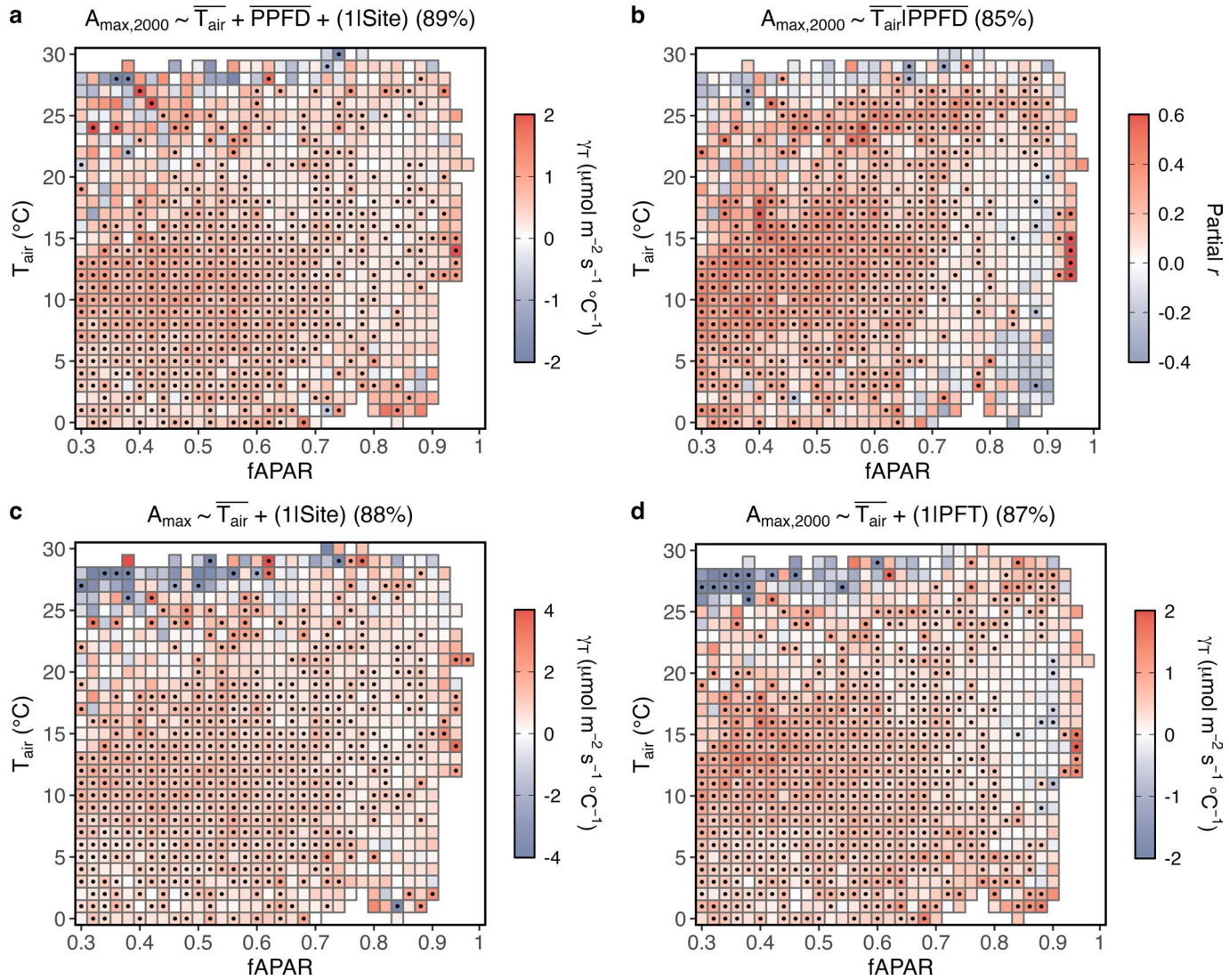

Extended Data Fig. 2 | The relationships between canopy photosynthetic capacities and $\overline{T_{air}}$ over fAPAR and T_{air} bins. a, The partial effect of $\overline{T_{air}}$ on $A_{max,2000}$ when $\overline{PPFD}$ is also incorporated in the modelling ($A_{max,2000} \sim \overline{T_{air}} + \overline{PPFD} + (1|Site)$). **b**, Partial correlation coefficients (partial *r*) between $A_{max,2000}$ and $\overline{T_{air}}$ when controlling for $\overline{PPFD}$ ($A_{max,2000} \sim \overline{T_{air}}|\overline{PPFD}$). **c**, The cross-site thermal acclimation rate (γ_T) is calculated based on A_{max} ($A_{max} \sim \overline{T_{air}} + (1|Site)$). **d**, The cross-site γ_T is calculated using plant function types (PFTs) as random intercepts ($A_{max,2000} \sim \overline{T_{air}} + (1|PFT)$). Numbers (%) in parentheses represent the detectability of positive γ_T values, which is defined as the percentage of the number of bins displaying a positive γ_T over the total number of bins. Black dots indicate significant ($P < 0.05$) correlations.

https://doi.org/10.1038/s41477-024-01846-1

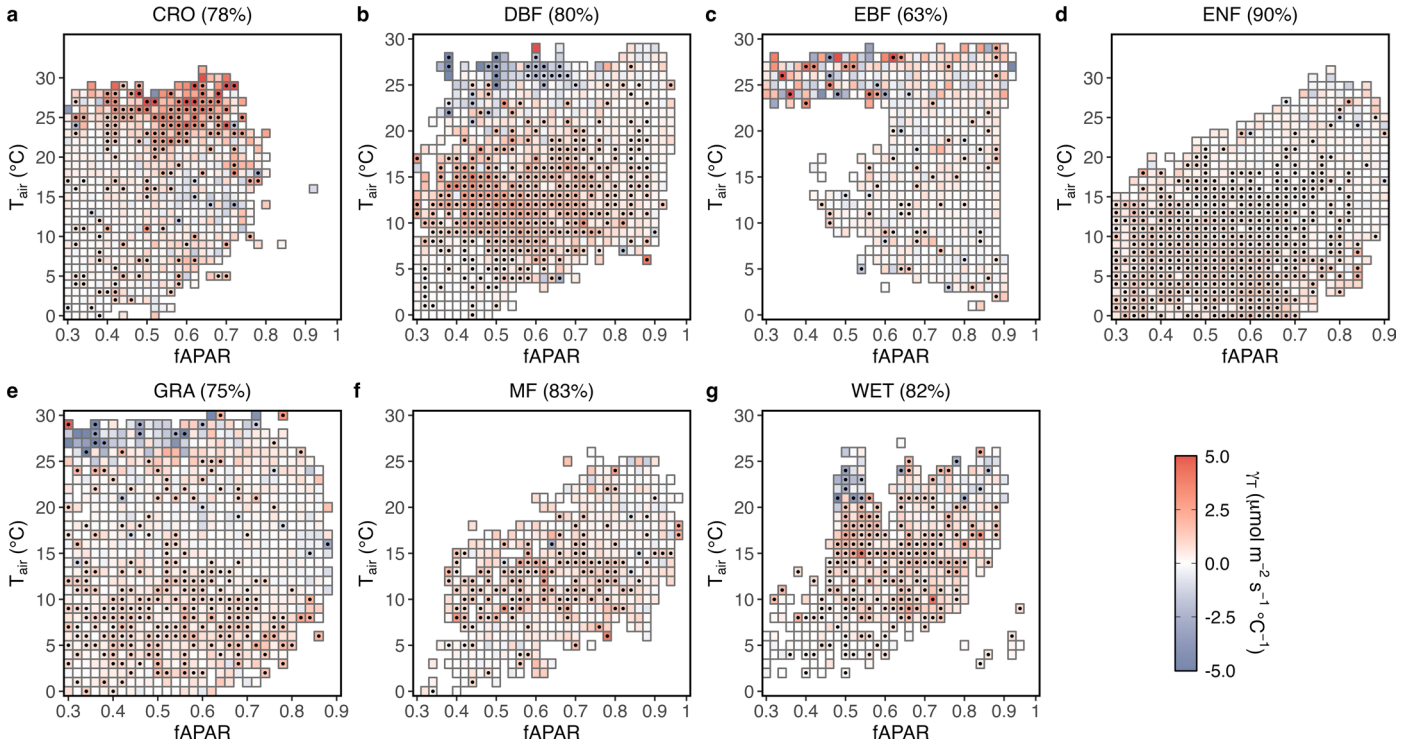

Extended Data Fig. 3 | The PFT-specific thermal acclimation rates (γ_T). a–g, PFT-specific γ_T for croplands (CRO) (**a**), deciduous broadleaf forests (DBF) (**b**), evergreen broadleaf forests (EBF) (**c**), evergreen needle-leaf forests (ENF) (**d**), grasslands (GRA) (**e**), mixed forests (MF) (**f**), wetlands (WET) (**g**). Numbers (%) in parentheses represent the detectability of positive γ_T values, which is defined as the percentage of the number of bins displaying a positive γ_T over the total number of bins. Black dots indicate significant ($P < 0.05$) correlations between $A_{max,2000}$ and $\overline{T_{air}}$.

https://doi.org/10.1038/s41477-024-01846-1

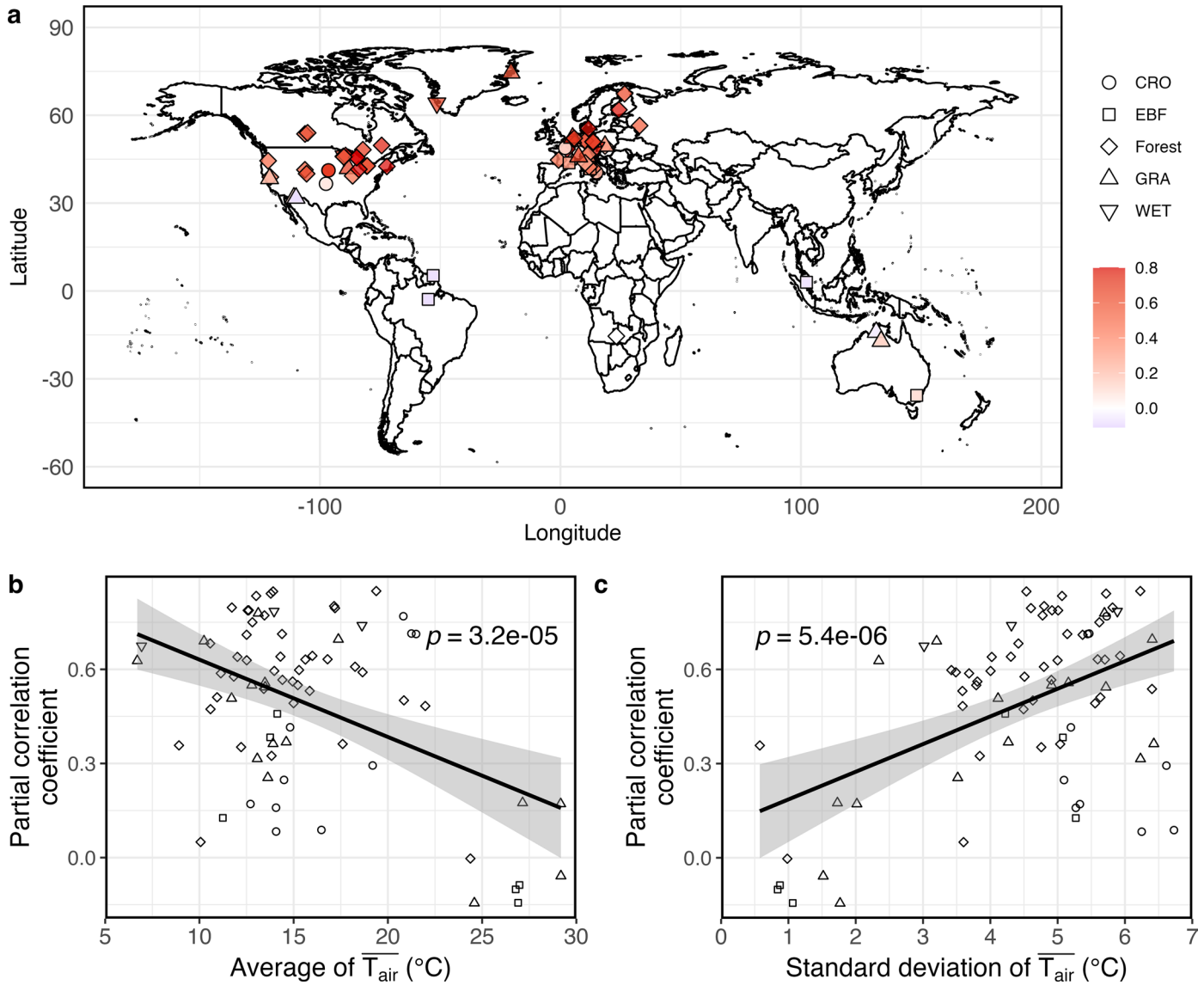

Extended Data Fig. 4 | Analyses of the partial correlation coefficients between $A_{max,2000}$ and $\overline{T_{air}}$ derived from long-term flux sites and their relationships with the site-level average $\overline{T_{air}}$ and variability of $\overline{T_{air}}$. **a**, Geographic distribution of partial correlation coefficients between $A_{max,2000}$ and $\overline{T_{air}}$ controlling for $\overline{PPFD}$, fAPAR and T_{air} across sites with observations spanning over five years. **b**, Relationship between partial correlation coefficients and the site-level averages of $\overline{T_{air}}$. **c**, Relationship between partial correlation coefficients and the site-level standard deviation of $\overline{T_{air}}$. The black lines in **b** and **c** represent the predicted mean values from linear regression models, and the grey shaded areas indicate their 95% confidence intervals. *P*-values are determined through two-sided Pearson's correlation significance tests. The "Forest" biome category includes evergreen needle-leaf forests, deciduous broadleaf forests, and mixed forests. Other PFTs are croplands (CRO), evergreen broadleaf forests (EBF), grasslands (GRA), and wetlands (WET).

nature portfolio

Corresponding author(s): Jiangong Liu
Youngryel Ryu

Last updated by author(s): Sep 28, 2024

Reporting Summary

Nature Portfolio wishes to improve the reproducibility of the work that we publish. This form provides structure for consistency and transparency in reporting. For further information on Nature Portfolio policies, see our Editorial Policies and the Editorial Policy Checklist.

Statistics

For all statistical analyses, confirm that the following items are present in the figure legend, table legend, main text, or Methods section.

n/a	Confirmed	
☐	☒	The exact sample size (*n*) for each experimental group/condition, given as a discrete number and unit of measurement
☐	☒	A statement on whether measurements were taken from distinct samples or whether the same sample was measured repeatedly
☐	☒	The statistical test(s) used AND whether they are one- or two-sided *Only common tests should be described solely by name; describe more complex techniques in the Methods section.*
☐	☒	A description of all covariates tested
☐	☒	A description of any assumptions or corrections, such as tests of normality and adjustment for multiple comparisons
☐	☒	A full description of the statistical parameters including central tendency (e.g. means) or other basic estimates (e.g. regression coefficient) AND variation (e.g. standard deviation) or associated estimates of uncertainty (e.g. confidence intervals)
☐	☒	For null hypothesis testing, the test statistic (e.g. *F*, *t*, *r*) with confidence intervals, effect sizes, degrees of freedom and *P* value noted *Give P values as exact values whenever suitable.*
☒	☐	For Bayesian analysis, information on the choice of priors and Markov chain Monte Carlo settings
☒	☐	For hierarchical and complex designs, identification of the appropriate level for tests and full reporting of outcomes
☐	☒	Estimates of effect sizes (e.g. Cohen's *d*, Pearson's *r*), indicating how they were calculated

Our web collection on statistics for biologists contains articles on many of the points above.

Software and code

Policy information about availability of computer code

Data collection	No software was used to collect data. All datasets are downloaded from the original sources.
Data analysis	All data analysis was conducted using R (version 4.2.1, program for statistical computing, www.R-project.org). Key R packages used in this study include ggplot2 (v3.5.1), lme4 (1.1.33), lmerTest(v3.1.3), ppcor (v1.1) and agricolae (v1.3.5). The code scripts for reproductivity have been archived on Zenodo: https://doi.org/10.5281/zenodo.13854273. The code for the deviation of Amax from the FLUXNET2015 database can be accessed at: https://github.com/trevorkeenan/inhibitionPaperCode. The code for modelling optimality-based Vcmax can be accessed at: https://github.com/chongya/SVOM.

For manuscripts utilizing custom algorithms or software that are central to the research but not yet described in published literature, software must be made available to editors and reviewers. We strongly encourage code deposition in a community repository (e.g. GitHub). See the Nature Portfolio guidelines for submitting code & software for further information.

Data

Policy information about availability of data

All manuscripts must include a data availability statement. This statement should provide the following information, where applicable:

- Accession codes, unique identifiers, or web links for publicly available datasets
- A description of any restrictions on data availability
- For clinical datasets or third party data, please ensure that the statement adheres to our policy

The dataset of FLUXNET2015 flux sites under the CC-BY-4.0 policy is publicly available for download at http://fluxnet.fluxdata.org. Remote-sensing canopy structure data from the MODIS MCD43A and MOD15A2H products are freely accessible at https://lpdaac.usgs.gov/products/mcd43a3v006/ and https://lpdaac.usgs.gov/products/mod15a2hv006/. BESS flux products are publicly available at https://www. environment.snu.ac.kr/data/. PFT-based Vcmax25C is derived from TRY trait database at https://www.try-db.org/TryWeb/dp.php.

Research involving human participants, their data, or biological material

Policy information about studies with human participants or human data. See also policy information about sex, gender (identity/presentation), and sexual orientation and race, ethnicity and racism.

Reporting on sex and gender	N/A
Reporting on race, ethnicity, or other socially relevant groupings	N/A
Population characteristics	N/A
Recruitment	N/A
Ethics oversight	N/A

Note that full information on the approval of the study protocol must also be provided in the manuscript.

Field-specific reporting

Please select the one below that is the best fit for your research. If you are not sure, read the appropriate sections before making your selection.

☐ Life sciences ☐ Behavioural & social sciences ☒ Ecological, evolutionary & environmental sciences

For a reference copy of the document with all sections, see nature.com/documents/nr-reporting-summary-flat.pdf

Ecological, evolutionary & environmental sciences study design

All studies must disclose on these points even when the disclosure is negative.

Study description	We derive Amax from light response curves of half-hourly or hourly eddy-covariance carbon fluxes obtained from more than 200 FLUXNET2015 flux sites. We examine the correlation between Amax and growth temperature when averaged over different time windows to identify the most relevant time scale for thermal acclimation, as indicated by peak correlation. Finally, we evaluate a biochemical model of canopy-scale C3 photosynthesis, incorporating recent advances in parameterizing temperature dependence acclimation and modelled optimality-based leaf photosynthetic capacity, to assess its ability to reproduce the observed thermal acclimation rates.
Research sample	Half-hourly and hourly net ecosystem exchanges of CO2 and their corresponding environmental conditions were collected from all sites listed on FLUXNET2015. MODIS LAI and fPAR data were also collected for each site.
Sampling strategy	We attempted to derived Amax from all FLUXNET2015 sites under the CC-BY-4.0 policy, though failed on three sites due to missing data variable and mismatched time periods with MODIS.
Data collection	All data were downloaded from their original source through the URLs provided in the data availability statement. The raw data were collected and processed by site PIs. The FLUXNET community standardized the flux data by ONEFlux.
Timing and spatial scale	We focused on the period between 2002 and 2014 when MODIS data were available and overlapped with FLUXNET2015. Daily fAPAR and LAI for each site were derived by interpolating the 8-day MODIS MOD15A2H products. We chose the growing seasons identified by fPAR and air temperature and well-watered conditions according to an aridity index (ET/PET).
Data exclusions	Sites are excluded if data are unavailable during the MODIS period from 2002 onwards (e.g. US-LWW and US-Me4) or if the uncertainty estimation is missing (e.g. CA-Man).

Reproducibility	Our analyses were based on the global eddy covariance database, public satellite products and well-documented methods. We provide the necessary data and code scripts to reproduce the results.
Randomization	Some of the results were grouped based on plant functional types, following the International Geosphere Biosphere Programme.
Blinding	Blinding does not apply as we studied natural terrestrial ecosystems.

Did the study involve field work? ☐ Yes ☒ No

Reporting for specific materials, systems and methods

We require information from authors about some types of materials, experimental systems and methods used in many studies. Here, indicate whether each material, system or method listed is relevant to your study. If you are not sure if a list item applies to your research, read the appropriate section before selecting a response.

Materials & experimental systems

n/a	Involved in the study
☒	☐ Antibodies
☒	☐ Eukaryotic cell lines
☒	☐ Palaeontology and archaeology
☒	☐ Animals and other organisms
☒	☐ Clinical data
☒	☐ Dual use research of concern
☐	☒ Plants

Methods

n/a	Involved in the study
☒	☐ ChIP-seq
☒	☐ Flow cytometry
☒	☐ MRI-based neuroimaging

Dual use research of concern

Policy information about dual use research of concern

Hazards

Could the accidental, deliberate or reckless misuse of agents or technologies generated in the work, or the application of information presented in the manuscript, pose a threat to:

No	Yes	
☒	☐	Public health
☒	☐	National security
☒	☐	Crops and/or livestock
☒	☐	Ecosystems
☒	☐	Any other significant area

Experiments of concern

Does the work involve any of these experiments of concern:

No	Yes	
☒	☐	Demonstrate how to render a vaccine ineffective
☒	☐	Confer resistance to therapeutically useful antibiotics or antiviral agents
☒	☐	Enhance the virulence of a pathogen or render a nonpathogen virulent
☒	☐	Increase transmissibility of a pathogen
☒	☐	Alter the host range of a pathogen
☒	☐	Enable evasion of diagnostic/detection modalities
☒	☐	Enable the weaponization of a biological agent or toxin
☒	☐	Any other potentially harmful combination of experiments and agents

Plants

Seed stocks	N/A
Novel plant genotypes	N/A
Authentication	N/A